

PRESSURE COMPARISON BETWEEN THE SPHERICAL CELLULAR MODEL AND THE THOMAS-FERMI MODEL

GEORGE A. BAKER, JR

*Los Alamos National Laboratory, Theoretical Division,
Los Alamos, NM 87545, USA
gbj@viking.lanl.gov*

The widely used Thomas Fermi model always produces pressure which is less than or equal to that of the ideal Fermi gas. On the other hand the spherical cellular model, in certain regions of the temperature-density plane, can produce pressures which are greater than that of the ideal gas. This phenomenon is investigated.

Keywords: Thomas-Fermi model; spherical cellular model.

1. Introduction

I have found an interesting feature of the pressure as produced by the spherical cellular model. Except for hydrogen, for low to moderate temperatures and densities, the pressure can exceed that of the ideal Fermi gas very significantly. It has been shown previously¹ that for certain types of attractive potentials that this result is possible. This effect is seen in the spherical cellular in part of the one-phase region. There is a physical explanation for this pressure phenomenon. As the electrons descend into the nuclear potential well, they move faster and faster which motion results in larger and larger momentum transfer at the surface of the sphere. That means that the pressure can be quite large.

On the other hand as I show, the pressure for the widely used Thomas-Fermi model. (See Figure 1.) is always less than or equal to that for the ideal gas. This disparity (Compare Figure 2 with Figure 1.) in theoretical results may have very significant effects in some practical applications. It is, I think, of considerable interest to resolve whether in actual physical systems this feature occurs.

The system under consideration is a partially ionized gas of nuclei of charge Ze where $-e$ is the electronic charge. I will compare two models of this system where each is confined to a finite sized sphere.

2. Thomas-Fermi Model

First the Thomas-Fermi theory² is given by

$$\rho = \int_0^\infty \frac{2 \times 4\pi p^2/h^3}{\exp[(p^2/2m - eV)/kT + \eta] + 1} dp, \tag{1}$$

where eV is the potential energy, It is convenient to define the auxiliary functions

$$I_n(\eta) = \int_0^\infty \frac{y^n}{\exp(y - \eta) + 1} dy. \tag{2}$$

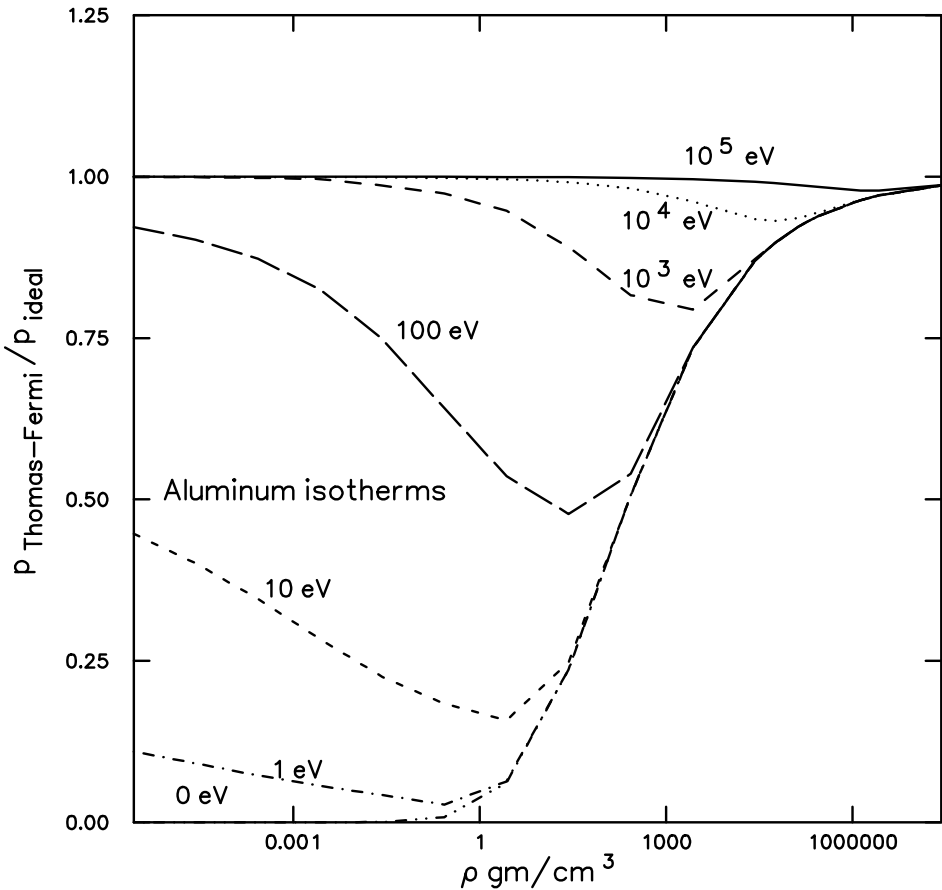


Fig. 1. The Thomas-Fermi model electron pressure divided by the ideal gas pressure vs. density for the case of Aluminum ($Z = 13$).

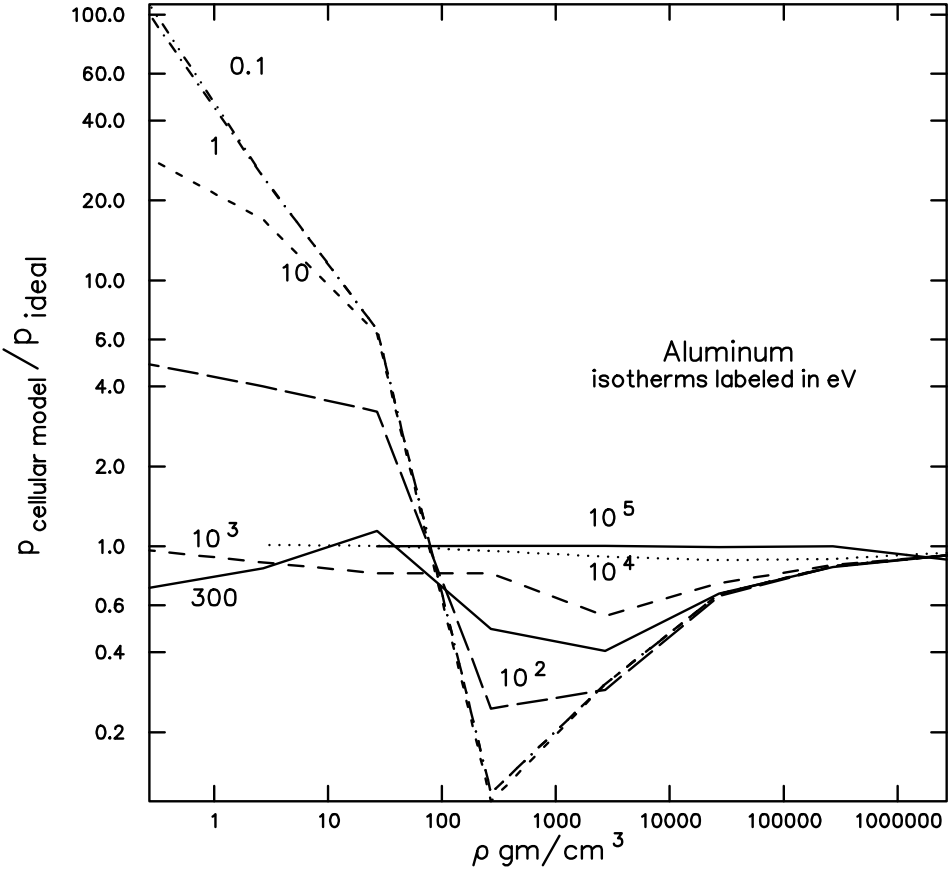


Fig. 2. The spherical cellular model electron pressure divided by the ideal gas pressure vs. density for the case of Aluminum ($Z = 13$). Notice that in Figure 1, the pressure is always less than the ideal pressure. Notice in Figure 2, for low densities and $T \leq 300$ eV the pressure can exceed the ideal.

The Poisson equation is then used to determine $V(r)$. It yields

$$\frac{1}{r} \frac{d^2}{dr^2} [rV(r)] = \frac{16\pi^2}{h^3} e(2mkT)^{1/2} I_{1/2}(eV(r)/kT - \eta). \tag{3}$$

The boundary conditions are $\lim_{r \rightarrow 0} rV(r) = Ze$ and the Z equals the integral of the density $\rho(r)$ over a sphere of radius r_b where $4\pi r_b^3 N/3 = \Omega$ where N is the number of atoms and Ω is the volume. The latter condition determines $\eta(T, r_b)$ The pressure is given by

$$\frac{p\Omega}{N} = \frac{32\pi^2 kT}{9} \left(\frac{2mkT}{h^2} \right)^{3/2} I_{3/2}(eV(r_b)/kT - \eta). \tag{4}$$

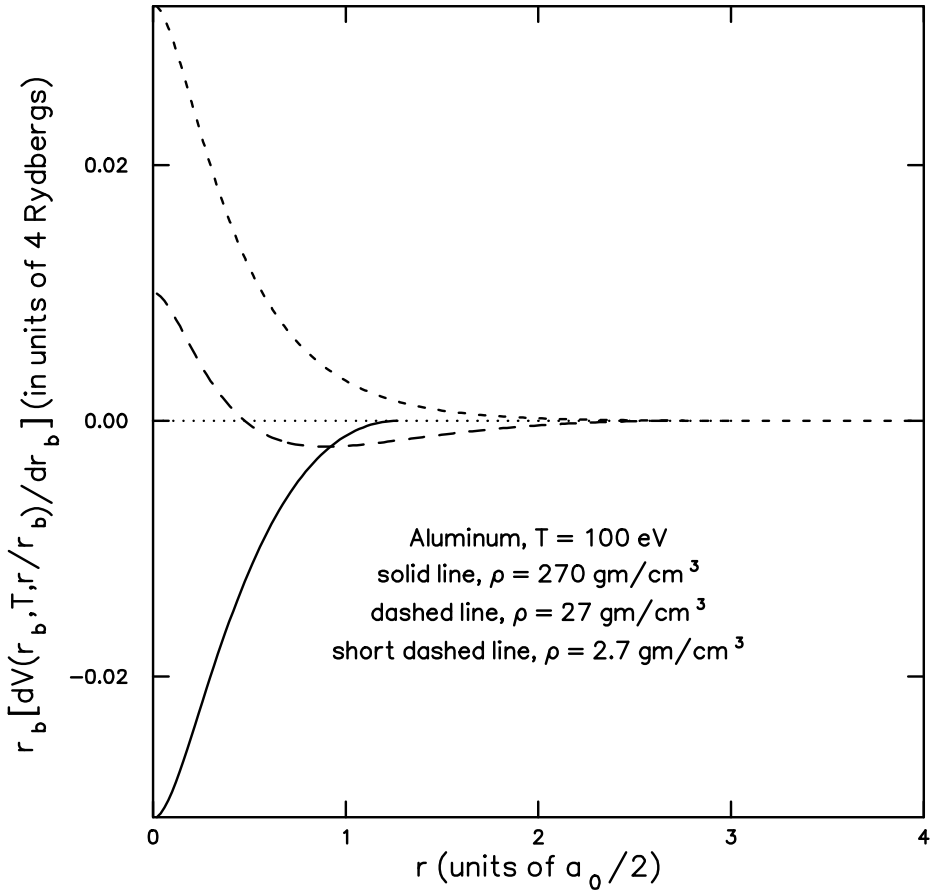


Fig. 3. $r_b \partial V(r_b, T, r/r_b)/\partial r_b|_T$ for the spherical cellular model as a function of r for the case of Aluminum ($Z = 13$).

Feynman, Metropolis and Teller³ have shown that the solution of these equations for any Z can be obtained from that for any other by means of similarity transformations.

3. Spherical Cellular Model

Next I describe, briefly, the spherical cellular model.⁴⁻⁶ First I remark for the ideal gas that, if space is divided into identical cubes, and if one sums over the eigenvalues in the cubes and integrates over the first Brillouin zone, then the exact result for the ideal gas is obtained. It is an approximation of a few percent to go to spherical cells instead.

The quantum statistical mechanics formulæ on which the usual formulation is

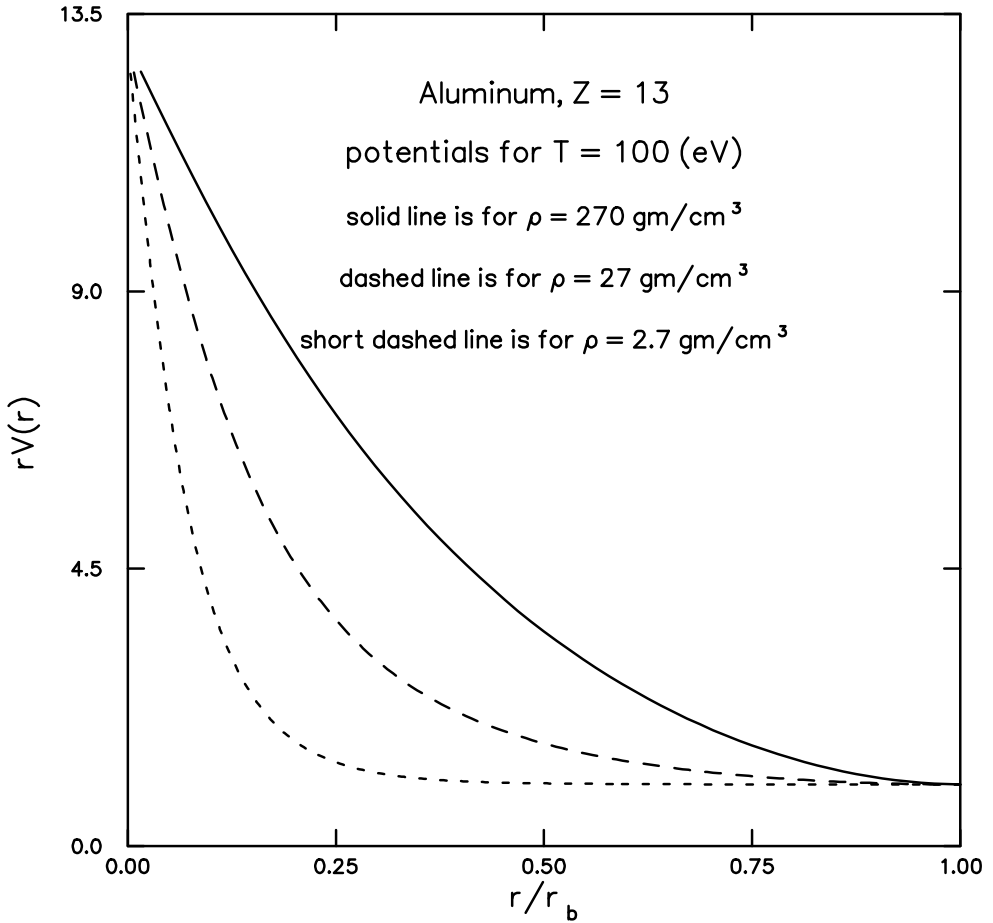


Fig. 4. The potentials $V(r_b, T, r/r_b)$ for the spherical cellular model as a function of r/r_b for the case of Aluminum ($Z = 13$).

based are given for Fermi-Dirac statistics.⁷ The grand canonical partition function is

$$\begin{aligned} \mathcal{Q}(\Omega, T) &= \sum_{N=0} \exp[N\mu(\Omega, T)/(kT)] Q_N(\Omega, T) \\ &= \prod_j \{1 + \exp[(\mu(\Omega, T) - \epsilon_j)/(kT)]\}. \end{aligned} \quad (5)$$

where the ϵ_j 's are the state energies. Differentiating by μ (the chemical potential), determines μ as the solution of

$$N = \sum_j \frac{1}{\exp[(\epsilon_j - \mu)/(kT)] + 1}, \quad (6)$$

where N is the average number of occupied states. The Helmholtz free energy is

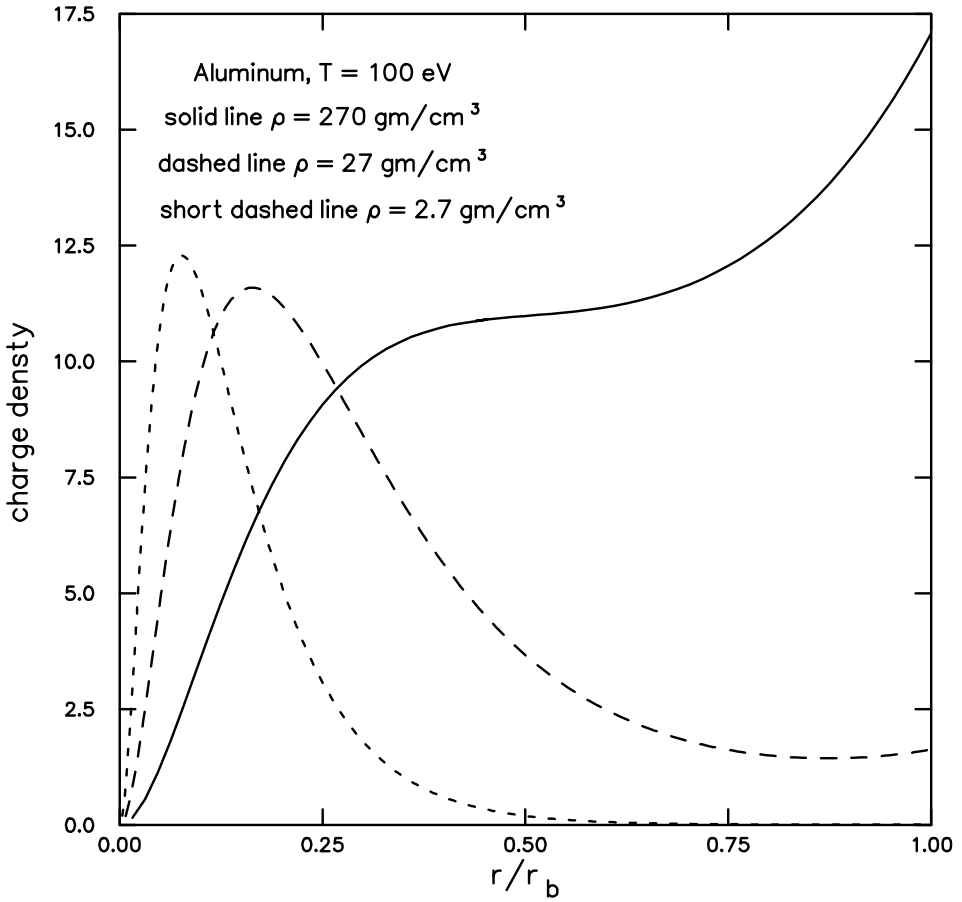


Fig. 5. The charge densities for several densities for the spherical cellular model as a function of r/r_b for the case of Aluminum ($Z = 13$).

then given as

$$A(\Omega, T) = \mathcal{N}\mu(\Omega, T) - kT \sum_j \ln\{1 + \exp[(\mu(\Omega, T) - \epsilon_j)/(kT)]\}. \quad (7)$$

From it, one can deduce the pressure as

$$p\Omega = -\frac{1}{3}r_b \left. \frac{\partial A}{\partial r_b} \right|_T = -\frac{1}{3} \sum_j \frac{r_b \left. \frac{\partial \epsilon_j}{\partial r_b} \right|_T}{\exp[(\epsilon_j - \mu)/(kT)] + 1}. \quad (8)$$

In order to make the calculations numerically feasible, I have introduced the independent electron approximation inside each atomic sphere.⁵ The Schrodinger equa-

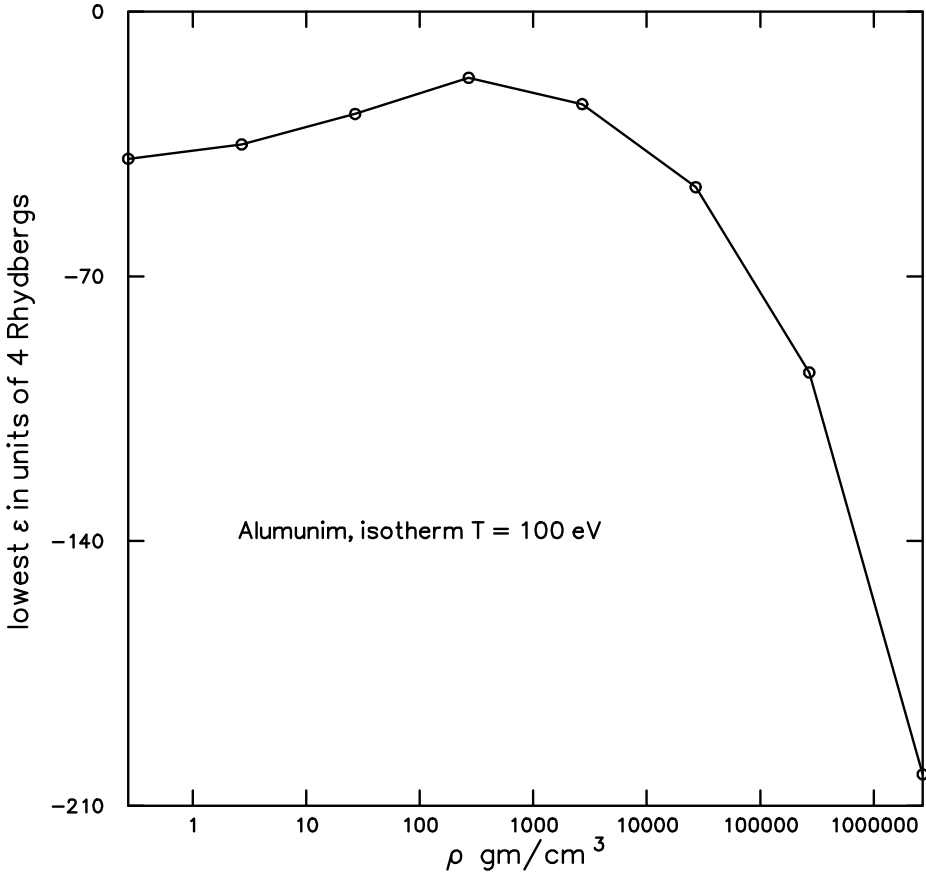


Fig. 6. The lowest $\epsilon(\vec{k} = \vec{0})$ vs. the density ρ .

tion to be solved is

$$\left\{ \frac{\hbar^2}{2m^*} \left[k^2 - 2i\vec{k} \cdot \vec{\nabla} - \nabla^2 \right] - \frac{e^2 Z^{-\frac{1}{3}} v(r_b, T, r/r_b)}{r} - \frac{e^2 Z^{-\frac{1}{3}}}{2r_b} \left(\frac{r}{r_b} \right)^2 F \left(\frac{y^2}{Z} \right) \right\} \phi_{l,\lambda}(\vec{r}) = \mathcal{E}_{l,\lambda}(\vec{k}) \phi_{l,\lambda}(\vec{r}), \tag{9}$$

with the boundary conditions

$$\vec{n} \cdot \vec{\nabla} \phi_{\text{even}}(Z^{\frac{1}{3}} \vec{r}_b) = 0, \quad \phi_{\text{odd}}(Z^{\frac{1}{3}} \vec{r}_b) = 0, \tag{10}$$

where \vec{n} is the unit vector normal to the sphere, and $y^2 = Ze^2/(r_b kT)$ is a dimensionless strength of the Coulomb interaction. \hat{r}_b is the radius of the spherical cell r_b over $Z^{1/3}$. The effective mass m^* is defined elsewhere.⁵ In the spherical cell approximation the normalization condition which determines the chemical potential

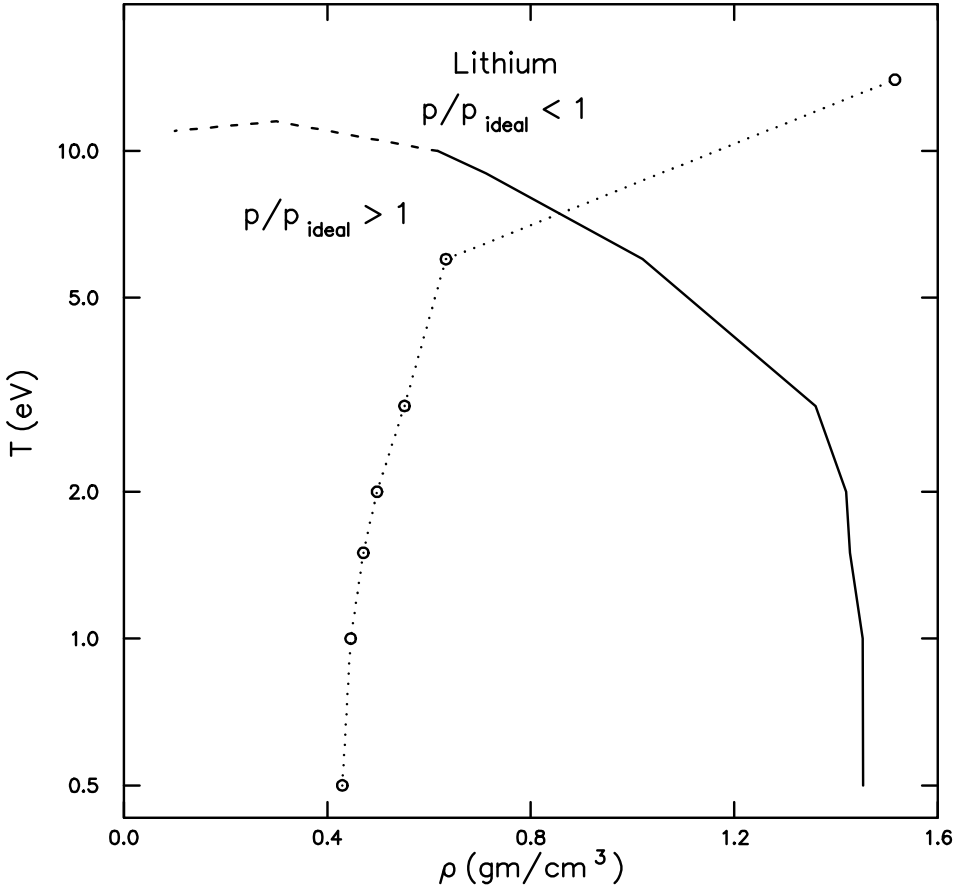


Fig. 7. The region where the electron pressure exceeds that of the ideal gas for the case of lithium ($Z = 3$). The dashed boundary is interpolated between two adjacent temperatures. The solid lines connect the data points. The dotted lines are (the straight lines connecting the data points on) the phase boundary. The open circles are those data points.

μ is

$$1 = 3 \sum_{l=0}^{\infty} (2l+1) \sum_{n=0}^{\infty} \int_0^1 d\hat{\kappa} \hat{\kappa}^2 \quad (11)$$

$$\times \left\{ \frac{1}{1 + \exp \left\{ (1.5\sqrt{\pi}\zeta)^{\frac{2}{3}} \left[e_{l,n} + \frac{1}{2} \left(1 + \frac{m^*}{m} \right) \left(\hat{\kappa}^2 + \hat{\kappa} \hat{\Delta}_{n+[(l+1)/2]} \right) \right] - \mu/kT \right\}} \right\}$$

$$+ \frac{1}{1 + \exp \left\{ (1.5\sqrt{\pi}\zeta)^{\frac{2}{3}} \left[e_{l,n} + \frac{1}{2} \left(1 + \frac{m^*}{m} \right) \left(\hat{k}^2 - \hat{k} \hat{\Delta}_{n+[(l+1)/2]} \right) \right] - \mu/kT \right\} \right\}},$$

where now the dimensionless form of the eigenvalue is, $e_{l,n} = 2m\epsilon_{l,n}(\vec{0})/(\hbar^2 k_B^2)$, where $k_B = (9\pi/2)^{1/3}/r_B$. The $\hat{\Delta}_{n+[(l+1)/2]}$ are defined elsewhere.⁵ For the corresponding ϵ ,

$$\begin{aligned} \epsilon_{l,\lambda}(\vec{k}) = & \frac{1}{2} \left(1 + \frac{m^*}{m} \right) \left[\mathcal{E}_{l,\lambda}(\vec{k}) - \frac{1}{2} \left\langle \phi_{l,\lambda}(\vec{r}) \left| \left(\frac{Z^{\frac{2}{3}} e^2}{r} - \frac{e^2 v(r_b, T, r/r_b) Z^{-\frac{1}{3}}}{r} \right) \phi_{l,\lambda}(\vec{r}) \right. \right\rangle \right] \\ & - \frac{1}{2} \left(1 - \frac{m^*}{m} \right) \left\langle \phi_{l,\lambda}(\vec{r}) \left| \frac{v(r_b, T, r/r_b) e^2 Z^{-\frac{1}{3}}}{r} \phi_{l,\lambda}(\vec{r}) \right. \right\rangle \\ & + \frac{m^* e^2 Z^{-\frac{1}{3}}}{4mr_b} F \left(\frac{y^2}{Z} \right) \left\langle \phi_{l,\lambda}(\vec{r}) \left| \frac{r^2}{r_b^2} \phi_{l,\lambda}(\vec{r}) \right. \right\rangle + \Delta\epsilon, \end{aligned} \tag{12}$$

where the state independent part is

$$\begin{aligned} \Delta\epsilon_{||} = & Z^{-\frac{1}{3}} \left\{ \frac{3e^2}{10r_b} g(y^2) + \frac{3Ze^2}{5r_b} F(y^2 Z) + \frac{e^2}{r_b} F \left(\frac{y^2}{Z} \right) \left[\frac{3}{4} - \left(\frac{3Z}{\pi\zeta} \right)^{\frac{1}{3}} f_{\frac{1}{2}}(z(\zeta)) \right] \right\}, \\ \Delta\epsilon_{\text{anti-}||} = & Z^{-\frac{1}{3}} \left\{ \frac{3e^2}{10r_b} g(y^2) + \frac{3Ze^2}{5r_b} F(y^2 Z) + \frac{3e^2}{4r_b} F \left(\frac{y^2}{Z} \right) \right\}. \end{aligned} \tag{13}$$

For the anti-parallel case $m^*/m = 1$ and I drop the $f_{\frac{1}{2}}$ term. m^* is the effective mass in the parallel spin case. Account has been taken of the double counting of the electron-electron interactions. The potential is determined self-consistently by the use of Poisson's equation which leads to

$$v(r_b, T, r/r_b) = 1 + \left(\frac{Z-1}{Z} \right) r_b \int_{(r/r_b)}^1 \left(1 - \frac{r}{\beta r_b} \right) \mathcal{D}(r_b, T, \beta) d\beta. \tag{14}$$

$\mathcal{D}(r_b, T, \beta)$ is the electron density. For the case of a uniform density $\mathcal{D}(r_b, T, r/r_b) = 3Zr^2/r_b^3$, and $v(r_b, T, r/r_b) = Z + \frac{1}{2}(Z-1)[(r/r_b)^3 - 3(r/r_b)]$. I use this value to start the iteration procedure to find the solution of these equations.

4. Pressure Comparison

Notice that in Figure 1, the pressure is always less than the ideal pressure. Notice in Figure 2, for low densities and $T \leq 300$ eV the pressure can exceed the ideal. Under current investigation is the point that the region where p/p_{ideal} is greater than 5 to 10 is either thermodynamically forbidden or in the two phase region. In either case, one would not expect reliable results from the spherical cellular model. The quantity plotted in Figure 3 is in the pressure equation and for positive values can increase the pressure above the ideal. Comparing Figures 4 and Figure 5 we see

that as the density decreases the peak of the electron density moves to progressively stronger values of the potential. Consequently the electrons move faster and faster. This motion is related to an increase in the pressure. For low temperatures the integral over the Brillouin zone gives the ideal gas pressure and the positive slope of ϵ as seen in Figure 6 adds to that pressure. Figure 7 shows the region where the pressure exceeds that of the ideal gas for the case of lithium ($Z = 3$).

The cellular model incorporates the following low temperature physics. Note that the pressures depend on the partial derivative of the state energies with respect to volume. At very high densities the lowest eigenvalue is very negative so that partial derivative is negative. As one reaches intermediate densities an atom like state is seen. Here the lowest eigenvalue decreases as the volume restriction is removed. The integration over the first Brillouin zone acts like the ideal-gas, kinetic energy and the change in the eigenvalue gives extra pressure. The physics here is complicated and the simple spherical cellular model may have over estimated this effect. Part, but not all, of the region in which the overpressure is seen in the spherical cellular model is thermally unstable as the internal energy decreases as the temperature increases. In aluminum for temperatures greater than 100 to 150 eV depending on the density, or less than a few eV or for a density greater than 27 gm/cm^3 the results are thermodynamically stable. At extreme dilutions, the entropy causes there to be full ionization so this limit for the spherical cellular model is again the ideal Fermi gas. The Thomas-Fermi model shows no such "overpressure."

DOES THIS "OVERPRESSURE" OCCUR IN REAL SYSTEMS?

There are some experimental results⁸ on aluminum for $\rho = 0.1, 0.3 \text{ gm/cm}^3$ at temperatures of a few eV. They indicate a system of very little ionization with the pressure less than that of an ideal gas of electrons and ions.

This work was carried out under the auspices of the National Nuclear Security Administration of the U. S. Department of Energy at the Los Alamos National Laboratory under Contract No. DE-AC52-06NA25396. The author is pleased to acknowledge a partial travel support from the U.S. Army Research Office. The views, opinions, and/or findings contained in this article, are those of the author and should not be construed as an official department of the army position, policy or decision, unless so designated by other documentation.

References

1. G. A. Baker, Jr., *J. Stat. Phys.* **110**, 971 (2003).
2. S. Eliezer, A. Ghatak, and H. Hora, *Fundamentals of Equations of State* (World Scientific, Singapore, 2002).
3. R. P. Feynman, N. Metropolis, and E. Teller, *Phys. Rev.* **75**, 1561 (1949).
4. G. A. Baker, Jr., *Phys. Rev. E* **56**, 5216 (1997).
5. G. A. Baker, Jr., *Phys. Rev. E* **68**, 056112 (2003).
6. G. A. Baker, Jr., to be published *Phys. Rev. E*.
7. K. Huang, *Statistical Mechanics* (Wiley, New York, 1963).
8. P. Renaudin, C. Blancard, J. Cl rouin, G. Faussurier, P. Noiret, and V. Recoules, *Phys. Rev. Lett.* **91**, 075002 (2003).